Journal of Zhejiang University-SCIENCE A (Applied Physics & Engineering) 2023 24(9):749-761
www.jzus.zju.edu.cn; www.springer.com/journal/11582
E-mail: jzus_a@zju.edu.cn

Research Article

https://doi.org/10.1631/jzus.A2300184

Finite-time path following control of a sailboat with actuator failure and unknown sideslip angle

Yujin WU[1], Kangjian SHAO[1], Ning WANG[2]✉, Zhongchao DENG[1]

[1]*Science and Technology on Underwater Vehicle Laboratory, Harbin Engineering University, Harbin 150001, China*
[2]*School of Marine Engineering, Dalian Maritime University, Dalian 116026, China*

Abstract: Suffering from actuator failure and complex sideslip angle, the motion control of a sailboat becomes challenging. In this paper, an improved double finite-time observer-based line-of-sight guidance and finite-time control (IDFLOS-FC) scheme is presented for path following of sailboats. The salient features of the proposed IDFLOS-FC scheme are as follows: (1) Considering the problem of actuator failure, an actuator failure model is introduced into the dynamics model of a sailboat. (2) The time-varying sideslip angle of the sailboat is accurately observed by the double finite-time sideslip observers (DFSOs), which reduces the error in line-of-sight (LOS) guidance. (3) A radial basis function (RBF) neural network is used to fit the uncertainty of the model, and the upper bound of the sum of fault effects and external disturbances is estimated based on adaptive theory, so that the controller has accurate tracking and interference suppression. (4) According to the Lyapunov method, the system is finite-time stable. Finally, simulation was used to validate the effectiveness of the method.

Key words: Sailboat; Sideslip angle; Sideslip angle observer; Finite-time control (FC); Path following

1 Introduction

Over recent decades, unmanned surface vehicles (USVs) have contributed greatly to marine military and commercial fields with their outstanding independent capabilities and excellent comprehensive performance (Manley, 2008; Liu et al., 2016; Wang et al., 2022). However, due to limitations, a traditional USV is not suitable for performing prolonged and complex tasks. An unmanned sailboat is assisted by wind, which reduces energy consumption and has significant advantages in performing large-scale and long-term tasks (Wang et al., 2019; Hong et al., 2020). Therefore, research on unmanned sailboats for marine exploration and improving maritime safety has great potential value.

An unmanned sailboat needs to be equipped with navigation and control systems to complete its autonomous navigation tasks. At present, research is carried out mainly around the platform body, navigation system, and control system of unmanned sailboats, which are interrelated and inseparable. The platform ontology provides the basic conditions for the autonomous navigation of unmanned sailboats, and the navigation system and control system play important roles in their autonomous missions.

In navigation, the conventional line-of-sight (LOS) guidance strategy is an effective navigation algorithm that has been widely used in USVs. Pettersen and Lefeber (2001) applied LOS to way-point tracking control. Liu et al. (2017) proposed an improved LOS guidance algorithm that can adjust adaptively according to the path tracking error. Li et al. (2023) integrated LOS guidance into the formation strategy under the leader-follower scheme and achieved good results. In actual navigation, unmanned sailboats are prone to sideslip, which is irregular and difficult to measure, and this adversely affects the accuracy of LOS guidance. Xia et al. (2019) proposed an LOS guidance law with large sideslip angle compensation to obtain the command heading angle signal for the control system. Liu (2022) designed an improved extended state observer-based LOS (ELOS) for estimating complex sideslip angle. A finite-time observer-based LOS was designed by Wang

✉ Ning WANG, n.wang@ieee.org
Ning WANG, https://orcid.org/0000-0003-1745-1425

Received Apr. 8, 2023; Revision accepted July 8, 2023;
Crosschecked Aug. 28, 2023

et al. (2018), in which the sideslip angle was accurately observed at short notice.

In terms of control, path following technology is crucial for the implementation of various key tasks, which determines the technical level and comprehensive performance of unmanned sailboats. For the convenience of calculation, most scholars ignored the roll motion of USVs (Wille et al., 2016; Viel et al., 2018; Dos Santos and Goncalves, 2019). However, due to the existence of sails, the roll response of unmanned sailboats needs to be considered. Xiao and Jouffroy (2014) proposed a four-degree-of-freedom (DOF) mathematical model of a keel-sailboat that took roll moment into consideration, but did not consider the influence of external disturbance. To ensure the accuracy of path following, the influence of external disturbance should be considered. Cui et al. (2016) summarized the external disturbance and model uncertainty as aggregate uncertainties and observed them using an adaptive disturbance observer with good results. Ma et al. (2021) presented an event-based switched USV control system to account for the simultaneous presence of communication delays, disturbance, faults, and denial-of-service (DoS) jamming attacks. Xu et al. (2020) used a radial basis function (RBF) neural network to estimate the external disturbance of a USV. In the control domain, accurate tracking of the desired path is a prerequisite and key for USVs to accomplish various tasks. For the trajectory tracking problem of marine aerial-surface heterogeneous (MASH) system, Wang and Ahn (2021) proposed a coordinated trajectory-tracking control (CTTC) scheme and obtained better tracking results. To solve the trajectory tracking problem of an asymmetric underactuated surface vehicle, Wang and Su (2021) designed a finite-time unknown observer-based interactive trajectory tracking control (FUO-ITTC) scheme, and the experimental results showed that the scheme has a good performance in both transient and steady state tracking. Wang et al. (2021) developed a novel reinforcement learning-based optimal tracking control (RLOTC) scheme for a USV in the presence of complex unknowns, including dead-zone input nonlinearities, system dynamics, and disturbances. Simulation results showed that the scheme has significant effectiveness and superiority.

An unmanned sailboat with solar power generation equipment can perform long-term operations at sea and can complete an information collection task well under the normal operation of the system. However, long-term work has led to the failure of some equipment. The presence of sails has caused great disturbance at sea. In particular, the rudder control actuator has to be adjusted according to the external environment, which increases the wear of the actuator. Therefore, it is necessary to study the fault-tolerant control of unmanned sailboats. At present, fault control of surface ships can be solved by robust control. An actuator robust fault-tolerant control method for a USV with unknown model and disturbance was proposed by Chen et al. (2016). Considering the failure of the USV's propulsion device, the actuator fault-tolerant controller was proposed in combination with the actuator configuration matrix and the change of the actuator configuration matrix caused by the rotatable propulsion device. Wang and Deng (2020) designed a finite-time fault estimation method using a finite-time observer and solved the USV trajectory tracking problem under an unknown actuator fault, input saturation, and uncertainty, and proved that the system error is finite-time convergent. Wan et al. (2022) designed a fixed-time observer to solve the unknown actuator failure problem, and a nonlinear fast fixed-time terminal sliding mode to improve the speed of system convergence. The system error showed fixed-time convergence. Qin et al. (2020) designed fault-tolerant control laws through tan-shaped Lyapunov functions to limit errors and improve the robustness of the system after actuator failure. Emami and Banazadeh (2020) studied the problem of USV trajectory tracking under sensor failure and designed a closed-loop system with fault-tolerant capability based on model predictive control. Fu et al. (2018) designed a time-varying sliding mode controller with neural network estimation for yaw angle and yaw speed oscillation caused by thruster faults and disturbances. Zhou et al. (2019) designed a network-based fault estimation scheme, which estimates the state and fault of a USV simultaneously in the network environment, and proposed a fault-tolerant controller based on a fault observer. For sailboats, the existing fault-tolerant controllers are gradually stable. In practice, the limited time stability can make sailboats quickly recover to a normal state in the case of actuator failure.

Inspired by the above academic results, this paper combines observer and LOS guidance to enhance the guidance accuracy, and designs the control law based on finite-time theory to realize the accurate tracking of

the sailboat on the desired path. The main contributions of this paper are as follows:

(1) The designed double finite-time sideslip observer (DFSO) compensates the time-varying sideslip angle in real time, thus improving the accuracy of LOS guidance.

(2) Finite-time filter is designed so as to avoid repeated derivation of the virtual control law.

(3) The fault model of the unmanned sailboat is considered, and a non-singular terminal sliding mode with adaptive parameter adjustment is designed to enhance the robustness of the system and prevent the system from leaving the equilibrium state when the actuator suddenly fails.

(4) Considering the problem of model uncertainty, the minimum parameter estimation method is used to estimate the uncertain part of the unmanned sailboat model, and a fault-tolerant control method for an unmanned sailboat based on an adaptive parameter adjustment sliding mode is designed. The error of the heading control system is proved to have finite-time convergence.

2 Problem formulations

As shown in Fig. 1 (Shao et al., 2023), the motion of an unmanned sailboat can be described in terms of body-referenced and inertial-referenced frames. ψ_{tw} and U_{tw} are true wind angle and velocity, respectively. $\{x_b, y_b, z_b\}$ denotes the body-referenced frame.

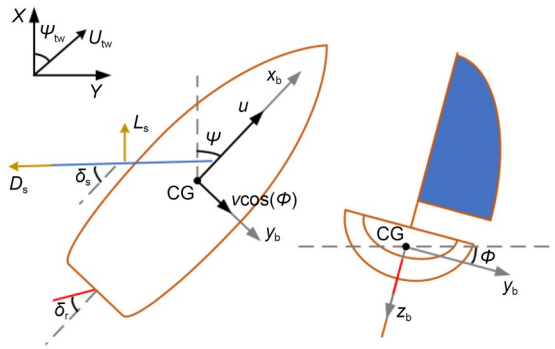

Fig. 1 Sailboat in different coordinates. Reprinted from (Shao et al., 2023), Copyright 2023, with permission from Springer Nature

The kinematic and dynamic model of a 4-DOF unmanned sailboat can be expressed as follows (Xiao and Jouffroy, 2014):

$$\begin{cases} \dot{x}=u\cos(\psi)-v\cos(\phi)\sin(\psi), \\ \dot{y}=u\sin(\psi)+v\cos(\phi)\cos(\psi), \\ \dot{\phi}=p, \\ \dot{\psi}=r\cos(\phi), \end{cases} \tag{1}$$

$$\begin{cases} m_u\dot{u}=F_{Su}+F_{Ru}-F_{Ku}+m_v vr-F_{Du}+d_{wu}, \\ m_v\dot{v}=F_{Sv}+F_{Rv}-F_{Kv}+m_u ur-F_{Dv}+d_{wv}, \\ m_p\dot{p}=M_{Sp}+M_{Rp}-M_{Kp}-c\,|\,p\,|p- \\ \qquad a\phi^2-b\phi-M_{Dp}+d_{wp}, \\ m_r\dot{r}=M_{Sr}+M_{Rr}-M_{Kr}-\left(X_{\dot{u}}-Y_{\dot{v}}\right)uv-M_{Dr}- \\ \qquad d\,|\,r\,|r\cos(\phi)+d_{wr}, \end{cases} \tag{2}$$

where (x, y, ϕ, ψ) denote the position vectors in inertial-referenced frame, and (u, v, p, r) denote the velocity vectors in body-referenced frame. $m_u=m-X_{\dot{u}}$, $m_v=m-Y_{\dot{v}}$, $m_p=I_{xx}-K_{\dot{p}}$, $m_r=I_{zz}-N_{\dot{r}}$, where m is the mass of sailboat, $X_{\dot{u}}$ and $Y_{\dot{v}}$ are additional masses, $K_{\dot{p}}$ and $N_{\dot{r}}$ are additional moments of inertia, and I_{xx} and I_{zz} are the moments of inertia along the x_b-axis and z_b-axis, respectively. a, b, c, and d are positive constants. F_{ij} and M_{ij} are force and torque (i=R, S, K, H, j=u, v, p, r), and R, S, K, and H represent rudder, sail, keel, and hull, respectively. d_{wi} (i=u, v, p, r) are forces generated by the external environment.

The attack angle α_s can be described as

$$\alpha_s=\alpha_w-\delta_s, \tag{3}$$

where α_w is the apparent wind angle, and δ_s is the sail angle.

The lift and drag forces of the sail L_s and D_s are

$$\begin{cases} L_s=\dfrac{1}{2}\rho_a A_s V_{as}^2 C_{Ls}(\alpha_s), \\ D_s=\dfrac{1}{2}\rho_a A_s V_{as}^2 C_{Ds}(\alpha_s), \end{cases} \tag{4}$$

where ρ_a is the density of air, A_s is the sail area, and V_{as} denotes the apparent wind speed. $C_{Ls}(\alpha_s)$ and $C_{Ds}(\alpha_s)$ are coefficients of lift and drag, respectively.

In this study, we ignore ocean current effects, so the attack angle of the rudder is $\alpha_r=-\delta_r$, where δ_r is the rudder angle. Then the moment produced by the rudder is

$$M_{Rr}=-\frac{1}{2}\rho_w A_r V_{ar}^2|\,x_r\,|C_{Lr}(-\delta_r), \tag{5}$$

where ρ_w is the density of seawater, A_r is the rudder area, and x_r denotes the projection of the rudder's center of gravity on the X-axis in the body-referenced frame. V_{ar} denotes the apparent rudder speed and $C_{Lr}(-\delta_r)$ denotes the lift coefficient of the rudder. Further details of the model can be found in (Xiao and Jouffroy, 2014).

3 Sideslip angle observation and LOS guidance

In order to observe the time-varying sideslip angle to improve the LOS guidance accuracy, double finite-time sideslip angle observers are designed in this section.

As shown in Fig. 2, the desired path is parameterized by a variable ω. The tangent angle of any point on the path can be described as $\psi_k=\arctan(\dot{y}_k/\dot{x}_k)$. $(x_k(\omega), y_k(\omega))$ is a point on the desired path, and (x,y) is the location of the sailboat. Define the position error of a sailboat as

$$\begin{bmatrix} x_e \\ y_e \end{bmatrix} = \begin{bmatrix} \cos(\psi_k) & \sin(\psi_k) \\ -\sin(\psi_k) & \cos(\psi_k) \end{bmatrix} \cdot \begin{bmatrix} x-x_k(\omega) \\ y-y_k(\omega) \end{bmatrix}. \tag{6}$$

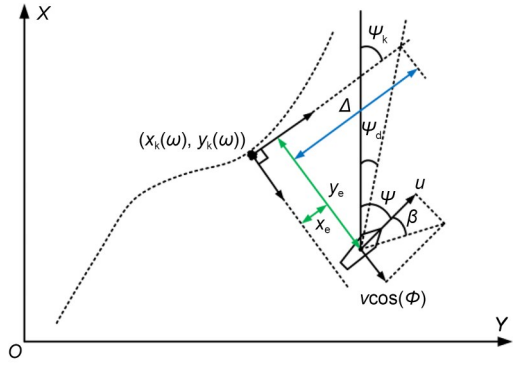

Fig. 2 Path following control geometry of a sailboat. Reprinted from (Shao et al., 2023), Copyright 2023, with permission from Springer Nature

The time derivative of Eq. (6) is

$$\begin{cases} \dot{x}_e = (\dot{x}-\dot{x}_k)\cos(\psi_k) + (\dot{y}-\dot{y}_k)\sin(\psi_k) + \dot{\psi}_k y_e, \\ \dot{y}_e = -(\dot{x}-\dot{x}_k)\sin(\psi_k) + (\dot{y}-\dot{y}_k)\cos(\psi_k) - \dot{\psi}_k x_e. \end{cases} \tag{7}$$

Substituting Eq. (1) into Eq. (7), we have

$$\begin{cases} \dot{x}_e = U\cos(\psi-\psi_k+\beta) + \dot{\psi}_k y_e - u_p, \\ \dot{y}_e = U\sin(\psi-\psi_k+\beta) - \dot{\psi}_k x_e, \end{cases} \tag{8}$$

where $U=\sqrt{u^2+[v\cos(\phi)]^2}$ is the combined speed of the sailboat, $\beta=\arctan[v\cos(\phi)/u]$ is the sideslip angle, and the velocity of the virtual target point is denoted by $u_p=\dot{\omega}\sqrt{\dot{x}_k^2+\dot{y}_k^2}$.

u_p is designed as

$$\begin{aligned} u_p &= U\cos\left(\psi-\psi_k+\hat{\beta}\right)+k_x x_e, \\ \dot{\omega} &= \frac{U\cos\left(\psi-\psi_k+\hat{\beta}\right)+k_x x_e}{\sqrt{\dot{x}_k^2+\dot{y}_k^2}}, \end{aligned} \tag{9}$$

where $k_x>0$.

Design the double finite-time sideslip angle observers as

$$\begin{cases} \dot{\hat{x}}_e = -\lambda_1 \operatorname{sig}^{\frac{4}{5}}(\tilde{x}_e) + \hat{h}_1 + \dot{\psi}_k y_e - u_p, \\ \dot{\hat{h}}_1 = -\lambda_2 \operatorname{sig}^{\frac{3}{5}}(\tilde{x}_e) + \vartheta_1 \operatorname{sign}(\tilde{x}_e), \end{cases} \tag{10}$$

$$\begin{cases} \dot{\hat{y}}_e = -\lambda_3 \operatorname{sig}^{\frac{4}{5}}(\tilde{y}_e) + \hat{h}_2 - \dot{\psi}_k x_e, \\ \dot{\hat{h}}_2 = -\lambda_4 \operatorname{sig}^{\frac{3}{5}}(\tilde{y}_e) + \vartheta_2 \operatorname{sign}(\tilde{y}_e), \end{cases} \tag{11}$$

where $h_1=U\cos(\psi-\psi_k+\beta)$, $h_2=U\sin(\psi-\psi_k+\beta)$, λ_i (i=1, 2, 3, 4), and ϑ_j (j=1, 2) are tuning parameters. Let $\tilde{x}_e=\hat{x}_e-x_e$, $\tilde{h}_1=\hat{h}_1-h_1$, $\tilde{y}_e=\hat{y}_e-y_e$, and $\tilde{h}_2=\hat{h}_2-h_2$, and then the time derivatives of $\tilde{x}_e$, $\tilde{h}_1$, $\tilde{y}_e$, and $\tilde{h}_2$ are

$$\begin{cases} \dot{\tilde{x}}_e = -\lambda_1 \operatorname{sig}^{\frac{4}{5}}(\tilde{x}_e) + \tilde{h}_1, \\ \dot{\tilde{h}}_1 = -\lambda_2 \operatorname{sig}^{\frac{3}{5}}(\tilde{x}_e), \end{cases} \tag{12}$$

$$\begin{cases} \dot{\tilde{y}}_e = -\lambda_3 \operatorname{sig}^{\frac{4}{5}}(\tilde{y}_e) + \tilde{h}_2, \\ \dot{\tilde{h}}_2 = -\lambda_4 \operatorname{sig}^{\frac{3}{5}}(\tilde{y}_e). \end{cases} \tag{13}$$

According to Lemma S3 in the electronic supplementary materials (ESM), there exists a time $T_{\beta 1}<5\left[V\left(\boldsymbol{\xi}_{\beta 1}(t_0)\right)\right]^{\frac{1}{5}}/\gamma_{\beta 1}$ so that $\tilde{x}_e\equiv 0$ and $\tilde{h}_1\equiv 0$, $\forall t\geqslant T_{\beta 1}$, where $V(\boldsymbol{\xi}_{\beta 1})=\boldsymbol{\xi}_{\beta 1}^{\mathrm{T}}\boldsymbol{P}_{\beta 1}\boldsymbol{\xi}_{\beta 1}$, $\boldsymbol{\xi}_{\beta 1}^{\mathrm{T}}=\left[\tilde{x}_e^{\frac{4}{5}},\ \tilde{h}_1^{\frac{3}{5}}\right]^{\mathrm{T}}$, $\gamma_{\beta 1}=\lambda_{\min}\left(\boldsymbol{Q}_{\beta 1}\right)/\lambda_{\max}\left(\boldsymbol{P}_{\beta 1}\right)$, satisfying $\boldsymbol{P}_{\beta 1}\boldsymbol{A}_{\beta 1}+\boldsymbol{A}_{\beta 1}^{\mathrm{T}}\boldsymbol{P}_{\beta 1}=-\boldsymbol{Q}_{\beta 1}$, and $\boldsymbol{A}_{\beta 1}=\begin{bmatrix} -\lambda_1 & 1 \\ -\lambda_2 & 0 \end{bmatrix}$. There also is a time $T_{\beta 2}<5\left[V\left(\boldsymbol{\xi}_{\beta 2}(t_0)\right)\right]^{\frac{1}{5}}/\gamma_{\beta 2}$, so that $\tilde{y}_e\equiv 0$ and $\tilde{h}_2\equiv 0$, $\forall t\geqslant T_{\beta 2}$, where $V(\boldsymbol{\xi}_{\beta 2})=$

$\boldsymbol{\xi}_{\beta 2}^{\mathrm{T}}\boldsymbol{P}_{\beta 2}\boldsymbol{\xi}_{\beta 2}$, $\boldsymbol{\xi}_{\beta 2}^{\mathrm{T}}=\left[\tilde{y}_{\mathrm{e}}^{\frac{4}{5}},\ \tilde{h}_2^{\frac{3}{5}}\right]^{\mathrm{T}}$, $\gamma_{\beta 2}=\lambda_{\min}(\boldsymbol{Q}_{\beta 2})/\lambda_{\max}(\boldsymbol{P}_{\beta 2})$, satisfying $\boldsymbol{P}_{\beta 2}\boldsymbol{A}_{\beta 2}+\boldsymbol{A}_{\beta 2}^{\mathrm{T}}\boldsymbol{P}_{\beta 2}=-\boldsymbol{Q}_{\beta 2}$, and $\boldsymbol{A}_{\beta 2}=\begin{bmatrix}-\lambda_3 & 1\\ -\lambda_4 & 0\end{bmatrix}$.

Remark 1 For $0<\kappa<1$, $\mathrm{sig}^{\kappa}(x)=|x|^{\kappa}\mathrm{sign}(x)$, where $\mathrm{sign}(x)$ is a sign function. For a given matrix $\boldsymbol{A}$, $\lambda_{\max}(\boldsymbol{A})$ denotes the largest eigenvalue of $\boldsymbol{A}$ and $\lambda_{\min}(\boldsymbol{A})$ denotes the smallest eigenvalue of $\boldsymbol{A}$.

The estimated value of the sideslip angle is

$$\hat{\beta}=\arcsin\left(\frac{\hat{h}_2\cos(\psi-\psi_{\mathrm{k}})-\hat{h}_1\sin(\psi-\psi_{\mathrm{k}})}{U}\right). \quad (14)$$

Then the error of sideslip angle is expressed as

$$\tilde{\beta}=\arcsin\left(\frac{\tilde{h}_2\cos(\psi-\psi_{\mathrm{k}})-\tilde{h}_1\sin(\psi-\psi_{\mathrm{k}})}{U}\right). \quad (15)$$

Therefore, the observed error of the sideslip angle converges to zero in finite time, when $t\geqslant\max\{T_{\beta 1}, T_{\beta 2}\}$, $\tilde{\beta}\equiv 0$.

The LOS method tracking angle is expressed as

$$\psi_{\mathrm{d}}=\psi_{\mathrm{k}}-\arctan\left(\frac{y_{\mathrm{e}}}{\Delta}\right)-\hat{\beta}, \quad (16)$$

where Δ is the look-ahead distance.

Substituting Eqs. (9) and (16) into Eq. (8), it can be obtained as

$$\begin{cases}\dot{x}_{\mathrm{e}}=-k_{\mathrm{x}}x_{\mathrm{e}}+\dot{\psi}_{\mathrm{k}}y_{\mathrm{e}},\\ \dot{y}_{\mathrm{e}}=-\dfrac{Uy_{\mathrm{e}}}{\sqrt{y_{\mathrm{e}}^2+\Delta^2}}\cos\left(\tilde{\beta}+\tilde{\psi}\right)-\dfrac{U\Delta}{\sqrt{y_{\mathrm{e}}^2+\Delta^2}}\sin\left(\tilde{\beta}+\tilde{\psi}\right)-\dot{\psi}_{\mathrm{k}}x_{\mathrm{e}}.\end{cases} \quad (17)$$

Choosing the Lyapunov function $V=\frac{1}{2}x_{\mathrm{e}}^2+\frac{1}{2}y_{\mathrm{e}}^2$, the derivative of V is as follows:

$$\begin{aligned}\dot{V}=&x_{\mathrm{e}}\dot{x}_{\mathrm{e}}+y_{\mathrm{e}}\dot{y}_{\mathrm{e}}=-k_{\mathrm{x}}x_{\mathrm{e}}^2+\dot{\psi}_{\mathrm{k}}y_{\mathrm{e}}x_{\mathrm{e}}-\\ &\frac{Uy_{\mathrm{e}}^2}{\sqrt{y_{\mathrm{e}}^2+\Delta^2}}\cos\left(\tilde{\beta}+\tilde{\psi}\right)-\frac{U\Delta y_{\mathrm{e}}}{\sqrt{y_{\mathrm{e}}^2+\Delta^2}}\sin\left(\tilde{\beta}+\tilde{\psi}\right)-\\ &\dot{\psi}_{\mathrm{k}}x_{\mathrm{e}}y_{\mathrm{e}}\leqslant-k_{\mathrm{x}}x_{\mathrm{e}}^2+2U_{\max}\left(|y_{\mathrm{e}}|+\Delta\right)=\\ &-k_{\mathrm{x}}x_{\mathrm{e}}^2-k_{\mathrm{x}}y_{\mathrm{e}}^2+2U_{\max}\left(|y_{\mathrm{e}}|+\Delta\right)+k_{\mathrm{x}}y_{\mathrm{e}}^2=\\ &-k_{\mathrm{x}}V+2U_{\max}\left(|y_{\mathrm{e}}|+\Delta\right)+k_{\mathrm{x}}y_{\mathrm{e}}^2,\end{aligned} \quad (18)$$

where $U_{\max}$ is the maximum of U. Consider the sets $\Omega_{\mathrm{s}}=\left\{(x_{\mathrm{e}},y_{\mathrm{e}})\,|\,x_{\mathrm{e}}^2+y_{\mathrm{e}}^2\leqslant\sigma_{\mathrm{s}}\right\}$, where $\sigma_{\mathrm{s}}>0$. Eq. (18) can be expressed by $\dot{V}\leqslant-k_{\mathrm{x}}V+u$, and $u=2U_{\max}\left(|y_{\mathrm{e}}|+\Delta\right)+k_{\mathrm{x}}y_{\mathrm{e}}^2$, which means that the system is asymptotically stable.

4 Heading control

4.1 Controller design

Considering heading control, Eqs. (1) and (2) can be simplified as

$$\begin{aligned}&\dot{\psi}=r\cos(\phi),\\ &m_r\dot{r}=M_{\mathrm{S}r}+M_{\mathrm{R}r}-M_{\mathrm{K}r}-\left(X_{\dot{u}}-Y_{\dot{v}}\right)uv-\\ &\qquad M_{\mathrm{H}r}-d\,|r|r\cos(\phi)+d_{\mathrm{w}r},\end{aligned} \quad (19)$$

where $M_{\mathrm{R}r}=F_{\mathrm{r}}\delta_{\mathrm{r}}$ and F_{r} is the rudder force. For the simplification of the rudder lift coefficient, please refer to Deng et al. (2020).

Considering the failure problem of the rudder actuator of the unmanned sailboat, we define $\delta_{\mathrm{r}}^{\mathrm{F}}$ as the rudder angle of the actuator failure, and the mathematical model of the actuator failure can be expressed by

$$\delta_{\mathrm{r}}^{\mathrm{F}}=(1-s)\,\delta_{\mathrm{r}}+\bar{\delta}_{\mathrm{r}}, \quad (20)$$

where s is the actuator loss efficiency and $\bar{\delta}_{\mathrm{r}}$ is the actuator foundation failure. According to the change of s and $\bar{\delta}_{\mathrm{r}}$, the actuator will have different degrees of failure. When $s=1$, the actuator rudder angle completely fails and does not have the ability to control the steering; when $0<s<1$, the actuator rudder angle partially fails, but still has some ability to control the steering; when $s=0$, the actuator rudder angle does not fail.

It is obtained from Eq. (5) that $M_{\mathrm{R}r}=-0.6\rho_{\mathrm{w}}A_{\mathrm{r}}V_{\mathrm{ar}}^2\times|x_{\mathrm{r}}|\sin(-2\delta_{\mathrm{r}})$. By bringing the mathematical model of the failure into the mathematical model of bow motion, the steering moment considering the actuator failure can be derived in the following form:

$$\begin{aligned}M_{\mathrm{R}r}=&\lambda\sin\left[-2\left((1-s)\,\delta_{\mathrm{r}}+\bar{\delta}_{\mathrm{r}}\right)\right]=\\ &\lambda\sin\left(-2\delta_{\mathrm{r}}+2s\delta_{\mathrm{r}}-2\bar{\delta}_{\mathrm{r}}\right)=\\ &\lambda\sin(-2\delta_{\mathrm{r}})\cos\left(2s\delta_{\mathrm{r}}-2\bar{\delta}_{\mathrm{r}}\right)+\\ &\lambda\cos(-2\delta_{\mathrm{r}})\sin\left(2s\delta_{\mathrm{r}}-2\bar{\delta}_{\mathrm{r}}\right)=\\ &\lambda\sin(-2\delta_{\mathrm{r}})+\lambda\sin(-2\delta_{\mathrm{r}})\left[\cos\left(2s\delta_{\mathrm{r}}-2\bar{\delta}_{\mathrm{r}}\right)-1\right]+\\ &\lambda\cos(-2\delta_{\mathrm{r}})\sin\left(2s\delta_{\mathrm{r}}-2\bar{\delta}_{\mathrm{r}}\right),\end{aligned} \quad (21)$$

where $\lambda=-0.6\rho_{\mathrm{w}}A_{\mathrm{r}}V_{\mathrm{ar}}^2|x_{\mathrm{r}}|$.

Therefore, the above equation allows us to write M_{Rr} as an effective steering moment term and a steering failure moment term:

$$M_{Rr}=M_{Rr}^{C}+M_{Rr}^{F}, \tag{22}$$

where $M_{Rr}^{F}=\lambda\sin(-2\delta_r)\left[\cos\left(2s\delta_r-2\bar{\delta}_r\right)-1\right]+\lambda\cos(-2\delta_r)\times\sin\left(2s\delta_r-2\bar{\delta}_r\right)$ represents the steering failure moment, and $M_{Rr}^{C}=\lambda\sin(-2\delta_r)$ represents the effective steering moment.

Considering the actual situation of the cruise, the following assumptions were made.

Assumption 1: The steering failure torque is bounded, i.e., there exists a normal number M such that $M_{Rr}^{F}\leqslant M$.

Bringing Eq. (22) into Eq. (19), the dynamics model of the heading motion of the unmanned sailboat can be written as

$$\begin{aligned}m_r\dot{r}=&M_{Sr}+M_{Rr}^{C}+M_{Rr}^{F}-M_{Kr}-\\&\left(X_{\dot{u}}-Y_{\dot{v}}\right)uv-M_{Hr}-d\,|r\,|r\cos(\phi)+d_{wr}.\end{aligned} \tag{23}$$

Define the heading tracking error as follows:

$$z_1=\psi-\psi_d. \tag{24}$$

The virtual control law α is designed according to the heading tracking error z_1 and the desired angular derivative $\dot{\psi}_d$ of the heading as follows:

$$\alpha=\frac{1}{\cos(\phi)}\left(-k_1z_1+\dot{\psi}_d-\beta_1\mathrm{sig}^{\gamma}(z_1)\right), \tag{25}$$

where k_1 and β_1 are positive regulation parameters, and γ is a constant with a value range of $0<\gamma<1$.

To improve the accuracy of the estimation of $\dot{\alpha}$, we designed a finite-time filter as

$$\begin{cases}\dot{\theta}=l,\\ l=-\zeta_1|\theta-\alpha|^{\frac{1}{2}}\mathrm{sign}(\theta-\alpha)+\sigma_1,\\ \dot{\sigma}_1=-\zeta_2\mathrm{sign}(\sigma_1-l),\end{cases} \tag{26}$$

where ζ_1 and ζ_2 are two positive regulation parameters. σ_1 is a transition variable. Defining θ as the filtered value of α , we have $\dot{\theta}=l$, and by Lemma S2 in the ESM, the virtual control law estimation error is finite-time stable.

The filter output error is defined as

$$y_r=\theta-\alpha. \tag{27}$$

Define the yaw rate error variable z_2 of the sailboat as

$$z_2=r-\theta. \tag{28}$$

The Lyapunov candidate function is selected according to the heading tracking error as

$$V_1=\frac{1}{2}z_1^2. \tag{29}$$

The derivative of the Lyapunov candidate function with respect to time yields

$$\begin{aligned}\dot{V}_1=&z_1(\dot{\psi}-\dot{\psi}_d)=\\&z_1\left[(z_2+y_r+\alpha)\cos(\phi)-\dot{\psi}_d\right]=\\&z_1z_2\cos(\phi)+z_1y_r\cos(\phi)-k_1z_1^2-\beta_1(z_1^2)^{\frac{\gamma+1}{2}}.\end{aligned} \tag{30}$$

In actual navigation, the heel angle satisfies $-\frac{\pi}{2}\leqslant\phi\leqslant\frac{\pi}{2}$, so $0<\cos(\phi)\leqslant1$, and then Eq. (30) can be written as

$$\dot{V}_1\leqslant z_1z_2+z_1y_r-k_1z_1^2-\beta_1(z_1^2)^{\frac{\gamma+1}{2}}. \tag{31}$$

According to Young's inequality, the following inequality holds:

$$\begin{cases}z_1z_2\leqslant\frac{1}{2}z_1^2+\frac{1}{2}z_2^2,\\ z_1y_r\leqslant\frac{1}{2}z_1^2+\frac{1}{2}y_r^2.\end{cases} \tag{32}$$

Then Eq. (31) can be expressed as

$$\begin{aligned}\dot{V}_1\leqslant&\frac{1}{2}z_1^2+\frac{1}{2}z_2^2+\frac{1}{2}z_1^2+\frac{1}{2}y_r^2-k_1z_1^2-\beta_1(z_1^2)^{\frac{\gamma+1}{2}}=\\&-(k_1-1)z_1^2-\beta_1(z_1^2)^{\frac{\gamma+1}{2}}+\frac{1}{2}z_2^2+\frac{1}{2}y_r^2.\end{aligned} \tag{33}$$

Considering the large tracking error generated after the failure of the sailboat actuator, a robust sliding mode controller with adaptive regulation parameters was designed by simplifying some of the regulation

parameters and adding an integral term according to Guo et al. (2021). The adaptive regulation parameters were designed to make faster convergence to the sliding mode surface, and the fault-tolerant controller was designed using adaptive parameters.

The sliding surface was designed as

$$s=z_2+\int_0^t a_1\mathrm{sig}^{\kappa_1}(z_2(\tau))+a_2\mathrm{sig}^{\kappa_2}(z_2(\tau))\,\mathrm{d}\tau, \quad (34)$$

where $a_1=\dfrac{\eta}{\chi+(\omega_1-\chi)\,\mathrm{e}^{-\beta_2|\psi_\mathrm{e}|}}$, $a_2=\dfrac{\eta}{\chi+(\omega_2-\chi)\,\mathrm{e}^{\beta_2|\psi_\mathrm{e}|}}$, $\eta>0$, $\kappa_1>1$, $0<\kappa_2<1$, $\beta_2>1$, $\omega_1>\eta$, and $\omega_2<\eta$.

In this sliding surface, two adaptive parameters were designed to regulate the sliding mode. When the heading tracking deviation is large, a_1 will converge to $\dfrac{\eta}{\chi}$ and a_2 will converge to 0, and at this time, $a_1\mathrm{sig}^{\kappa_1}(z_2)$ plays the main role in the control. When the heading tracking error is small, a_1 will converge to $\dfrac{\eta}{\omega_1}$ and a_2 will converge to $\dfrac{\eta}{\omega_2}$, and at this time, $a_2\mathrm{sig}^{\kappa_2}[z_2(\tau)]$ plays its main role in the control, which ensures the rapidity of convergence and the robustness of the system.

In the heading dynamics model, $f(\cdot)$ is difficult to obtain exactly. In this study, we considered the model uncertainty and used a neural network for approximation.

$$f(\cdot)=\boldsymbol{W}^{\mathrm{T}}\boldsymbol{H}(\boldsymbol{x})+\varepsilon, \quad (35)$$

where $\boldsymbol{x}=[\psi,\ r,\ \phi]^{\mathrm{T}}$ is the input to the neural network. $\boldsymbol{H}(\boldsymbol{x})=[h_1(x),\ h_2(x),\ \ldots,\ h_p(x)]$ is the activation function with Gaussian function as the candidate. p is the number of nodes in the hidden layer of the network, and the expression is $h_p(x)=\exp\left[-\dfrac{(\boldsymbol{x}-\boldsymbol{c}_j)^{\mathrm{T}}(\boldsymbol{x}-\boldsymbol{c}_j)}{2b_j^2}\right]$, $j=1,\ 2,\ \ldots,\ p$, where $\boldsymbol{c}_j\in\mathbb{R}^3$ is the center of the receptive field and $\boldsymbol{b}_j\in\mathbb{R}^3$ is the width of the Gaussian function. $\boldsymbol{W}$ is the ideal weight matrix, and ε is the estimated error.

The uncertainty term is expressed as

$$f(\cdot)=M_{Sr}-M_{Kr}-\left(X_{\dot u}-Y_{\dot v}\right)uv-M_{Dr}-d|r|r\cos(\phi). \quad (36)$$

Directly using the RBF neural network to approximate the uncertainty term, the weight matrix needs to be learned online in real time, and the computation is large. To solve the problem of the large computation of the neural network, the minimum parameter method is used instead of a neural network algorithm, as follows:

$$\vartheta=\|\boldsymbol{W}\|^2. \quad (37)$$

Define the one-parameter adaptive law as

$$\dot{\hat\vartheta}=\mu\left[\frac{1}{2}s^2\boldsymbol{H}^{\mathrm{T}}(\boldsymbol{x})\boldsymbol{H}(\boldsymbol{x})-\sigma\hat\vartheta\right], \quad (38)$$

where μ and σ are positive constants.

Define the error $\tilde\vartheta=\hat\vartheta-\vartheta$, and estimate the upper bound on the sum of fault effects and external disturbances based on adaptive theory. Design $\varphi=M^2$, and then the estimated error is: $\tilde\varphi=\hat\varphi-\varphi$. The adaptive law is designed as

$$\dot{\hat\varphi}=\phi_0\left(\frac{s^2}{2\lambda^2}-\phi_1\hat\varphi\right), \quad (39)$$

where ϕ_0 and ϕ_1 are constants, $\phi_0>0$ and $\phi_1>0$.

In summary, the rudder angle control law for the design of an unmanned sailboat is

$$\alpha_\mathrm{M}=\left[\dot\theta-a_1\mathrm{sig}^{\kappa_1}(z_2)-a_2\mathrm{sig}^{\kappa_2}(z_2)-k_2s-k_3\mathrm{sig}^{\gamma}(s)\right]m_r-\frac{1}{2}s\boldsymbol{H}^{\mathrm{T}}(\boldsymbol{x})\boldsymbol{H}(\boldsymbol{x})-\frac{\hat\varphi s}{2\lambda^2}, \quad (40)$$

$$\delta_\mathrm{r}'=\arcsin\left(\frac{2\alpha_\mathrm{M}}{-1.2\rho_\mathrm{w}A_\mathrm{r}V_\mathrm{ar}^2|x_\mathrm{r}|}\right), \quad (41)$$

where k_2 and k_3 are two positive regulation parameters. The rudder angle rotation limit is set as

$$\delta_\mathrm{r}=\begin{cases}\delta_\mathrm{r}', & |\delta_\mathrm{r}'|<\dfrac{\pi}{6},\\ \dfrac{\pi}{6}\mathrm{sign}(\delta_\mathrm{r}'), & |\delta_\mathrm{r}'|\geqslant\dfrac{\pi}{6}.\end{cases} \quad (42)$$

4.2 Stability analysis

Design the Lyapunov candidate function as follows:

$$V_2=\frac{1}{2}s^2+\frac{1}{2\mu}\tilde\vartheta^2+\frac{1}{2\phi_0}\tilde\varphi^2. \quad (43)$$

The derivative of the Lyapunov candidate function with respect to time yields

$$\dot{V}_2 = s\dot{s} + \frac{1}{\mu}\tilde{\vartheta}\dot{\hat{\vartheta}} + \frac{1}{\phi_0}\tilde{\varphi}\dot{\hat{\varphi}} = s\left[\dot{r} - \dot{\theta} + a_1 \mathrm{sig}^{\kappa_1}(z_2) + a_2 \mathrm{sig}^{\kappa_2}(z_2)\right] + \tilde{\vartheta}\left[\frac{1}{2}s^2 \boldsymbol{H}^{\mathrm{T}}(x)\boldsymbol{H}(x) - \sigma\hat{\vartheta}\right] + \tilde{\varphi}\left(\frac{s^2}{2\lambda^2} - \phi_1\hat{\varphi}\right). \tag{44}$$

Bringing in the heading control law, the following inequality is obtained:

$$\dot{V}_2 \leqslant -k_2 s^2 - k_3 (s^2)^{\frac{\gamma+1}{2}} - \sigma\tilde{\vartheta}\hat{\vartheta} - \phi_1\tilde{\varphi}\hat{\varphi}. \tag{45}$$

According to Young's inequality, the following equations hold:

$$-\sigma\tilde{\vartheta}\hat{\vartheta} = -\sigma\tilde{\vartheta}\left(\tilde{\vartheta} + \vartheta\right) \leqslant -\sigma\tilde{\vartheta}^2 + \frac{\sigma}{2}\tilde{\vartheta}^2 + \frac{\sigma}{2}\vartheta^2 = -\frac{\sigma}{2}\tilde{\vartheta}^2 + \frac{\sigma}{2}\vartheta^2 = -\frac{\sigma}{4}\tilde{\vartheta}^2 - \frac{\sigma}{4}\left[\left|\tilde{\vartheta}\right| - \left(\tilde{\vartheta}^2\right)^{\frac{\gamma}{2}}\right]^2 + \frac{\sigma}{4}\left(\tilde{\vartheta}^2\right)^{\gamma} - \frac{\sigma}{2}\left(\tilde{\vartheta}^2\right)^{\frac{\gamma+1}{2}} + \frac{\sigma}{2}\vartheta^2 \leqslant -\frac{\sigma}{4}\tilde{\vartheta}^2 - \frac{\sigma}{2}\left(\tilde{\vartheta}^2\right)^{\frac{\gamma+1}{2}} + \frac{\sigma}{4}\left(\tilde{\vartheta}^2\right)^{\gamma} + \frac{\sigma}{2}\vartheta^2, \tag{46}$$

$$-\phi_1\tilde{\varphi}\hat{\varphi} = -\phi_1\tilde{\varphi}(\tilde{\varphi} + \varphi) \leqslant -\phi_1\tilde{\varphi}^2 + \frac{\phi_1}{2}\tilde{\varphi}^2 + \frac{\phi_1}{2}\varphi^2 = -\frac{\phi_1}{2}\tilde{\varphi}^2 + \frac{\phi_1}{2}\varphi^2 = -\frac{\phi_1}{4}\tilde{\varphi}^2 - \frac{\phi_1}{4}\left[|\tilde{\varphi}| - (\tilde{\varphi}^2)^{\frac{\gamma}{2}}\right]^2 + \frac{\phi_1}{4}(\tilde{\varphi}^2)^{\gamma} - \frac{\phi_1}{2}(\tilde{\varphi}^2)^{\frac{\gamma+1}{2}} + \frac{\phi_1}{2}\varphi^2 \leqslant -\frac{\phi_1}{4}\tilde{\varphi}^2 - \frac{\phi_1}{2}(\tilde{\varphi}^2)^{\frac{\gamma+1}{2}} + \frac{\phi_1}{4}(\tilde{\varphi}^2)^{\gamma} + \frac{\phi_1}{2}\varphi^2. \tag{47}$$

In summary, it can be obtained that

$$\dot{V}_2 \leqslant -k_2 s^2 - \frac{\sigma}{4}\tilde{\vartheta}^2 - \frac{\phi_1}{4}\tilde{\varphi}^2 - k_3 (s^2)^{\frac{\gamma+1}{2}} - \frac{\sigma}{2}\left(\tilde{\vartheta}^2\right)^{\frac{\gamma+1}{2}} - \frac{\phi_1}{2}(\tilde{\varphi}^2)^{\frac{\gamma+1}{2}} + \frac{\sigma}{4}\left(\tilde{\vartheta}^2\right)^{\gamma} + \frac{\sigma}{2}\vartheta^2 + \frac{\phi_1}{4}(\tilde{\varphi}^2)^{\gamma} + \frac{\phi_1}{2}\varphi^2. \tag{48}$$

Design the Lyapunov function as

$$V_3 = V_1 + V_2 = -(k_1 - 1)z_1^2 - k_2 s^2 - \frac{\sigma}{4}\tilde{\vartheta}^2 - \frac{\phi_1}{4}\tilde{\varphi}^2 - \beta_1 (z_1^2)^{\frac{\gamma+1}{2}} - k_3 (s^2)^{\frac{\gamma+1}{2}} - \frac{\sigma}{2}\left(\tilde{\vartheta}^2\right)^{\frac{\gamma+1}{2}} - \frac{\phi_1}{2}(\tilde{\varphi}^2)^{\frac{\gamma+1}{2}} + \frac{1}{2}z_2^2 + \frac{1}{2}y_{\mathrm{r}}^2 + \frac{\sigma}{4}\left(\tilde{\vartheta}^2\right)^{\gamma} + \frac{\sigma}{2}\vartheta^2 + \frac{\phi_1}{4}(\tilde{\varphi}^2)^{\gamma} + \frac{\phi_1}{2}\varphi^2. \tag{49}$$

For a heading control system, there exists a constant $\sigma_s>0$, such that the system error satisfies the set $\left\{z_1^2 + z_2^2 + y_{\mathrm{r}}^2 + s^2 + \tilde{\vartheta}^2 + \tilde{\varphi}^2 \leqslant 2\sigma_s\right\}$, then there exists a constant c_1, such that $c_1 > \frac{1}{2}z_2^2 + \frac{1}{2}y_{\mathrm{r}}^2 + \frac{\sigma}{4}\left(\tilde{\vartheta}^2\right)^{\gamma} + \frac{\sigma}{2}\vartheta^2 + \frac{\phi_1}{4}(\tilde{\varphi}^2)^{\gamma} + \frac{\phi_1}{2}\varphi^2$, then Eq. (49) can be simplified as

$$\dot{V}_3 \leqslant -a_3 V_3 - b_1 V_3^{\frac{\gamma+1}{2}} + c_1, \tag{50}$$

where $a_3 = \min\left\{k_1 - 1,\ k_2,\ \frac{\sigma}{4},\ \frac{\phi_1}{4}\right\}$ and $b_1 = \min\left\{\beta_1 \cdot 2^{\frac{\gamma+1}{2}},\ k_3 \cdot 2^{\frac{\gamma+1}{2}},\ \sigma \cdot 2^{\frac{\gamma-1}{2}},\ \varphi \cdot 2^{\frac{\gamma-1}{2}}\right\}$. Therefore, according to Lemma 1 in the ESM, it can be proved that the error of the unmanned sailboat heading system is finite time stable.

When the system error is calibrated to the sliding surface, we have $s(t)\equiv 0$ and $\dot{s}(t)\equiv 0$, then

$$\dot{z}_2 = -a_1 \mathrm{sig}^{\kappa_1}(z_2) - a_2 \mathrm{sig}^{\kappa_2}(z_2). \tag{51}$$

Therefore, the convergence of the system is discussed when the error is stabilized to the sliding mode surface. The Lyapunov candidate function is defined as

$$V_4 = \frac{1}{2}z_2^2. \tag{52}$$

The derivative of V_4 yields

$$\dot{V}_4 = -z_2\left[a_1 \mathrm{sig}^{\kappa_1}(z_2) + a_2 \mathrm{sig}^{\kappa_2}(z_2)\right] = -a_1 \mathrm{sig}^{\kappa_1+1}(z_2) - a_2 \mathrm{sig}^{\kappa_2+1}(z_2). \tag{53}$$

V_4 is bounded when t tends to infinity, and then we have

$$\frac{1}{2}z_2^2 = V_4 < \infty. \tag{54}$$

In addition, the following inequalities are given by

$$\begin{aligned} |z_2|^{1+\kappa_1} &\leqslant |z_2|^2 + 1, \\ |z_2|^{1+\kappa_2} &\leqslant |z_2|^3 + 1. \end{aligned} \tag{55}$$

We have

$$\begin{aligned} |z_2|^{\frac{1+\kappa_1}{2}} &\leqslant \sqrt{2V_4 + 1} < \infty, \\ |z_2|^{\frac{1+\kappa_2}{2}} &\leqslant \sqrt{2V_4^{\frac{3}{2}} + 1} < \infty. \end{aligned} \tag{56}$$

From Eq. (53), we can obtain:

$$\int_0^t |z_2|^{1+\kappa_1} + |z_2|^{1+\kappa_2} \mathrm{d}\tau = V_4(0) - V_4(t) < \infty. \quad (57)$$

Therefore, combining Eqs. (56) and (57), from Barbalat's theorem, we have

$$\lim_{t\to\infty} z_2(t) = 0. \quad (58)$$

The control algorithm in this study is shown in Fig. 3. When the unmanned sailboat is subject to external interference caused by wind and waves, and the rudder actuator has a failure that will reduce its performance, the controller respectively designs the adaptive adjustment parameter sliding mode and fault-tolerant adaptive items to compensate for the actuator failure and external disturbance. This improves the robustness of the actuator in case of its failure, and achieves a more accurate path following control.

5 Simulation studies

To demonstrate the feasibility and effectiveness of the proposed improved double finite-time observer-based line-of-sight guidance and finite-time control (IDFLOS-FC) scheme, simulation study is conducted on the sailboat. To reflect more realistic working conditions, we have added wind and wave disturbance forces (Fossen, 2011). The wind speed was set to 5 m/s and the wind angle was set to 5°. The height of the meaningful wave was set to 0.7 m, and the desired path is designed as

$$\begin{cases} x_k(\omega) = 70\sin(0.01\omega) + 0.7\omega, \\ y_k(\omega) = 0.7\omega. \end{cases} \quad (59)$$

The hydrodynamic parameters were chosen as follows: m=25900 kg, I_{zz}=24760 kg·m^2, ρ_w=1025 kg/m^3, A_r=1.17 m^2, and x_r=−8.2 m. The initial position of the unmanned sailboat in the simulation was (−25 m, 0 m), the initial longitudinal velocity was 1 m/s, and the initial values of the remaining states were set to zero. The control parameters were set to: k_x=0.1, λ_1=4, λ_2=40, λ_3=4, λ_4=40, ϑ_1=0.05, ϑ_2=0.05, Δ=30, ζ_1=0.09, ζ_2=0.001, k_1=0.4, k_2=0.2, k_3=0.1, η=0.9, χ=0.5, ω_1=2, ω_2=0.5, β_2=30, κ_1=1.5, κ_2=0.5, μ=5, σ=0.01, ϕ_0=2, ϕ_1=0.01, and λ=0.5.

Next, to verify the control effect of the controller designed in this study under the condition of actuator failure, we designed two test schemes as follows:

Scheme 1: The rudder actuator fails at 80 s, and the fault factor suddenly changes from 0 to 0.4, and an additional failure $\bar{\delta}_r = \frac{\pi}{60}\cos(0.1t)$ is generated at the same time. Set the wind direction to due north.

Scheme 2: The rudder actuator fails at 80 s, and the fault factor suddenly changes from 0 to 0.8, and an additional failure $\bar{\delta}_r = \frac{\pi}{10}\cos(0.1t)$ is generated at the same time. The wind direction is set to $\frac{\pi}{600}t$.

5.1 Simulation results of Scheme 1

The simulation results are shown in Figs. 4–10. The simulation effect of path following is shown in Fig. 4, which shows that the designed IDFLOS-FC scheme quickly converged to the desired path in about 20 s, and had high path following accuracy. Fig. 5 shows the control performance of the unmanned sailboat after the effect of the actuator rudder failure. Both the lateral and longitudinal errors of IDFLOS-FC are stabilized in a short time. Fig. 6 shows that the designed DFSO has good observation of the time-varying sideslip angle. Fig. 7 shows the heading tracking error

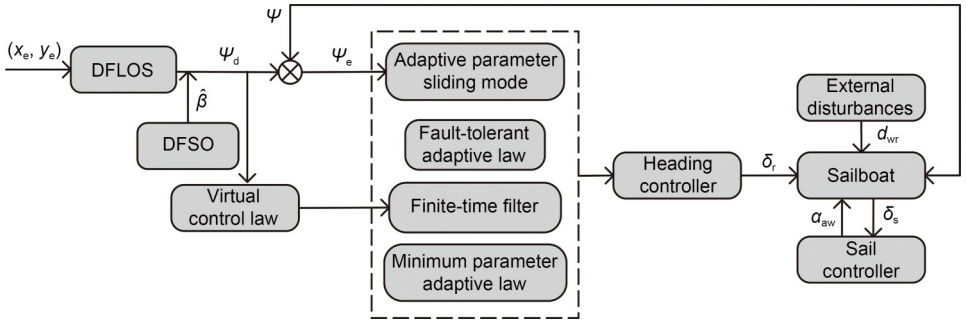

Fig. 3 Framework of sailboat control

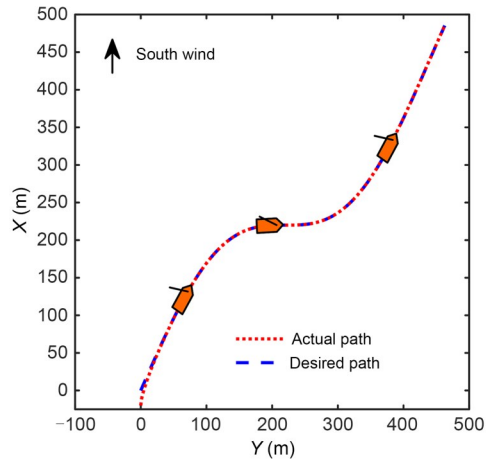

Fig. 4 Path following performance of the sailboat

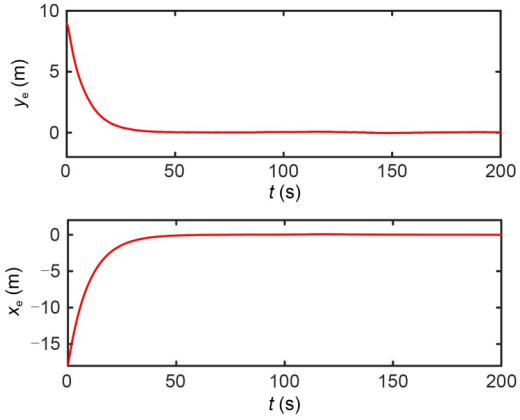

Fig. 5 Path tracking error (x_e, y_e)

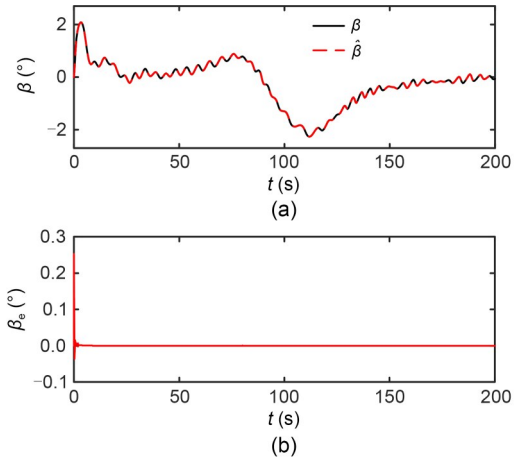

Fig. 6 Estimation (a) and error (b) of the sideslip angle

converged to 0 at about 10 s. Fig. 8 shows the curve of the rudder angle over time and Fig. 9 shows the curve of the sail angle over time. Fig. 10 shows the change of roll angle with time. The maximum roll angle of

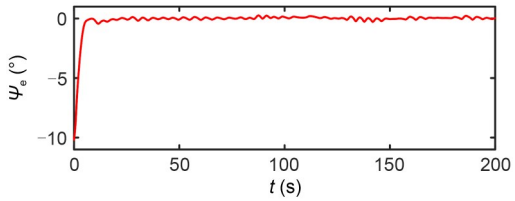

Fig. 7 Heading angle tracking error

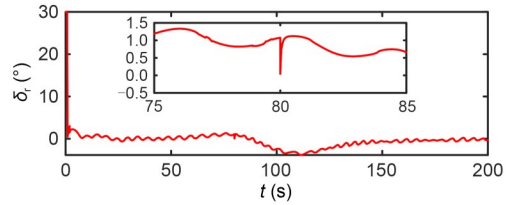

Fig. 8 Control input δ_r

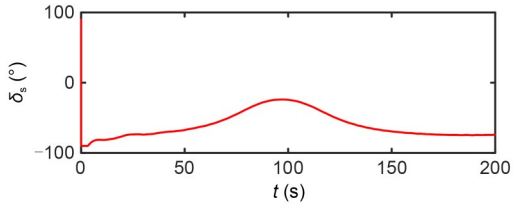

Fig. 9 Control input δ_s

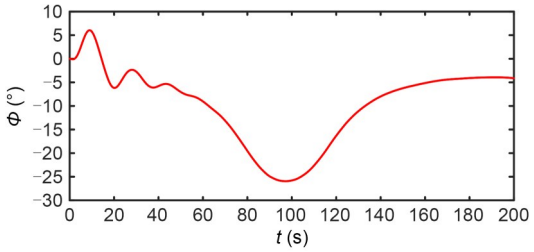

Fig. 10 Variation of sailboat roll angle

the sailboat did not exceed 30°, which is in line with the actual navigation.

5.2 Simulation results of Scheme 2

The simulation results are shown in Figs. 11–17. Fig. 11 shows that the designed IDFLOS-FC scheme can accurately track the desired path even if a fault is added. Fig. 12 shows that the lateral and longitudinal errors of the designed IDFLOS-FC scheme converged to zero in about 50 s. Fig. 13 shows that the designed DFSO accurately observed the sideslip angle even when the fault was increased. The heading tracking error converged to 0 in about 10 s (Fig. 14). After increasing the fault, the heading tracking deviated, but still

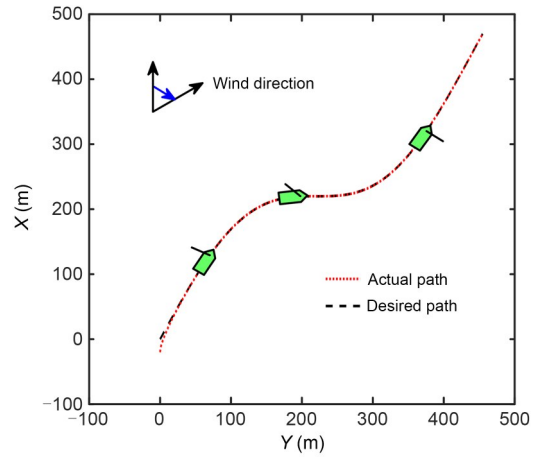

Fig. 11 Path following performance of the sailboat of Scheme 2

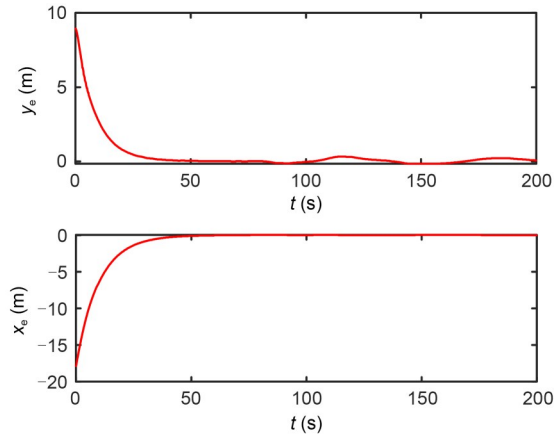

Fig. 12 Path tracking error (x_e, y_e) of Scheme 2

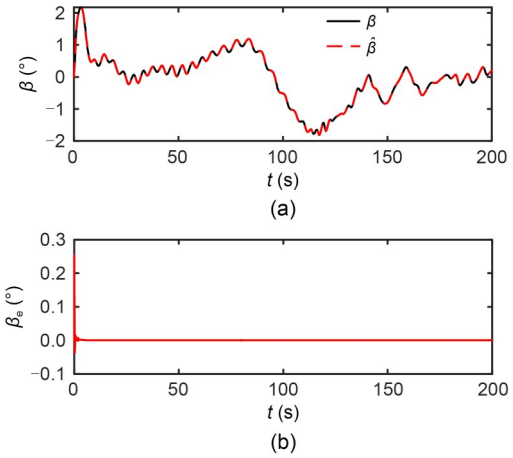

Fig. 13 Estimation (a) and error (b) of the sideslip angle of Scheme 2

maintained good tracking ability under the control law. Fig. 15 and Fig. 16 show the curves of the rudder angle and sail angle over time, respectively. Fig. 17 shows the change of roll angle with time, which was in line with the actual navigation.

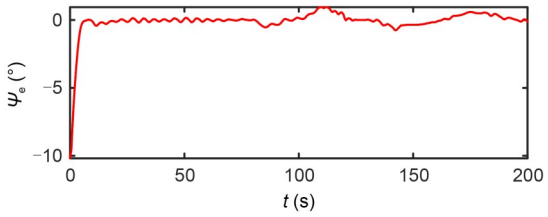

Fig. 14 Heading angle tracking error of Scheme 2

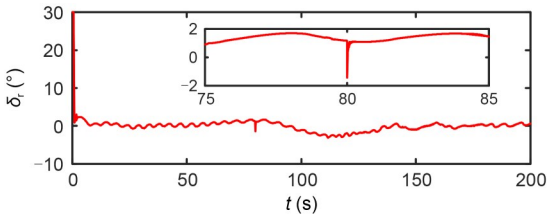

Fig. 15 . Control input δ_r of Scheme 2

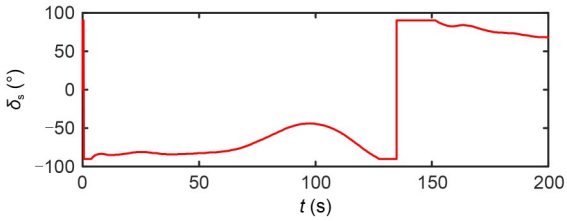

Fig. 16 Control input δ_s of Scheme 2

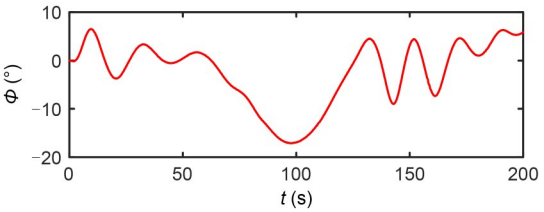

Fig. 17 Variation of sailboat roll angle of Scheme 2

In summary, the overall IDFLOS-FC scheme can achieve exact path following together with accurate sideslip angle observation in the presence of actuator failure, time-varying sideslip angle, and unknown external disturbances.

6 Conclusions

In this study, an IDFLOS-FC scheme was designed to solve the problem of controlling the path following

of a USV in the case of actuator failure and under the influence of a time-varying sideslip angle and unknown external disturbance. With the help of DFSO, the time-varying sideslip angle is accurately observed. A sliding model with adaptive parameter adjustment was designed. The sum of fault torque and disturbance force is estimated by an adaptive method, and the uncertain part of the model is estimated by a minimum parameter estimation method. Combining the backstepping method with finite-time theory, a finite-time controller based on DFLOS was established to stabilize the path following error and heading following error in finite-time. Simulation results show that the proposed IDFLOS-FC scheme can achieve accurate path following of an unmanned sailboat under the condition of actuator failure, time-varying sideslip angle, and unknown external disturbance, and can accurately track the desired path when adding faults. These results demonstrate the reliability and superiority of the IDFLOS-FC scheme.

Acknowledgments

This work is supported by the National Natural Science Foundation of China (Nos. 52271306, 52025111, and 51939003), the Central Guidance on Local Science and Technology Development Fund (No. 2023JH6/100100010), and the Fundamental Research Funds for the Central Universities (No. 3132023501), China.

Author contributions

Yujin WU designed the research. Yujin WU and Kangjian SHAO processed the corresponding data. Yujin WU wrote the first draft of the manuscript. Ning WANG and Zhongchao DENG helped to organize the manuscript. Yujin WU and Ning WANG revised and edited the final version.

Conflict of interest

Yujin WU, Kangjian SHAO, Ning WANG, and Zhongchao DENG declare that they have no conflict of interest.

References

Chen M, Jiang B, Cui RX, 2016. Actuator fault-tolerant control of ocean surface vessels with input saturation. *International Journal of Robust and Nonlinear Control*, 26(3): 542-564. https://doi.org/10.1002/rnc.3324

Cui RX, Zhang X, Cui D, 2016. Adaptive sliding-mode attitude control for autonomous underwater vehicles with input nonlinearities. *Ocean Engineering*, 123:45-54. https://doi.org/10.1016/j.oceaneng.2016.06.041

Deng YJ, Zhang XK, Zhang GQ, 2020. Line-of-sight-based guidance and adaptive neural path-following control for sailboats. *IEEE Journal of Oceanic Engineering*, 45(4): 1177-1189. https://doi.org/10.1109/JOE.2019.2923502

Dos Santos DH, Goncalves LMG, 2019. A gain-scheduling control strategy and short-term path optimization with genetic algorithm for autonomous navigation of a sailboat robot. *International Journal of Advanced Robotic Systems*, 16(1): 172988141882183. https://doi.org/10.1177/1729881418821830

Emami SA, Banazadeh A, 2020. Fault-tolerant predictive trajectory tracking of an air vehicle based on acceleration control. *IET Control Theory & Applications*, 14(5):750-762. https://doi.org/10.1049/iet-cta.2019.0596

Fossen TI, 2011. Handbook of Marine Craft Hydrodynamics and Motion Control. John Wiley & Sons Ltd., Chichester, UK.

Fu MY, Li MY, Xie WB, 2018. Finite-time trajectory tracking fault-tolerant control for surface vessel based on time-varying sliding mode. *IEEE Access*, 6:2425-2433. https://doi.org/10.1109/ACCESS.2017.2783319

Guo B, Chen Y, Zhou AJ, 2021. Event trigger-based adaptive sliding mode fault-tolerant control for dynamic systems. *Science China Information Sciences*, 64(6):169205. https://doi.org/10.1007/s11432-019-2681-1

Hong SM, Ha KN, Kim JY, 2020. Dynamics modeling and motion simulation of USV/UUV with linked underwater cable. *Journal of Marine Science and Engineering*, 8(5): 318. https://doi.org/10.3390/jmse8050318

Li Y, Li XW, Wei XW, 2023. Sim-real joint experimental verification for an unmanned surface vehicle formation strategy based on multi-agent deterministic policy gradient and line of sight guidance. *Ocean Engineering*, 270:113661. https://doi.org/10.1016/j.oceaneng.2023.113661

Liu T, Dong ZP, Du HW, 2017. Path following control of the underactuated USV based on the improved line-of-sight guidance algorithm. *Polish Maritime Research*, 24(1):3-11. https://doi.org/10.1515/pomr-2017-0001

Liu ZQ, 2022. Improved ELOS based path following control for underactuated surface vessels with roll constraint. *Ocean Engineering*, 245:110348. https://doi.org/10.1016/j.oceaneng.2021.110348

Liu ZX, Zhang YM, Yu X, et al., 2016. Unmanned surface vehicles: an overview of developments and challenges. *Annual Reviews in Control*, 41:71-93. https://doi.org/10.1016/j.arcontrol.2016.04.018

Ma Y, Nie ZQ, Hu SL, et al., 2021. Fault detection filter and controller co-design for unmanned surface vehicles under DoS attacks. *IEEE Transactions on Intelligent Transportation Systems*, 22(3):1422-1434. https://doi.org/10.1109/TITS.2020.2970472

Manley JE, 2008. Unmanned surface vehicles, 15 years of development. OCEANS 2008, p.1-4. https://doi.org/10.1109/OCEANS.2008.5289429

Pettersen KY, Lefeber E, 2001. Way-point tracking control of ships. Proceedings of the 40th IEEE Conference on Decision and Control, p.940-945.

https://doi.org/10.1109/CDC.2001.980230

Qin HD, Li CP, Sun YC, 2020. Adaptive neural network-based fault-tolerant trajectory-tracking control of unmanned surface vessels with input saturation and error constraints. *IET Intelligent Transport Systems*, 14(5):356-363. https://doi.org/10.1049/iet-its.2019.0221

Shao KJ, Wu YJ, Wang N, et al., 2023. Sailboat path following control based on LOS with sideslip angle observation and finite-time backstepping. S-Cube 2022: Sensor Systems and Software, p.63-78.

Viel C, Vautier U, Wan J, et al., 2018. Position keeping control of an autonomous sailboat. *IFAC-PapersOnLine*, 51(29): 14-19. https://doi.org/10.1016/j.ifacol.2018.09.462

Wan L, Cao Y, Sun YC, et al., 2022. Fault-tolerant trajectory tracking control for unmanned surface vehicle with actuator faults based on a fast fixed-time system. *ISA Transactions*, 130:79-91. https://doi.org/10.1016/j.isatra.2022.04.013

Wang N, Deng ZC, 2020. Finite-time fault estimator based fault-tolerance control for a surface vehicle with input saturations. *IEEE Transactions on Industrial Informatics*, 16(2): 1172-1181. https://doi.org/10.1109/TII.2019.2930471

Wang N, Ahn CK, 2021. Coordinated trajectory-tracking control of a marine aerial-surface heterogeneous system. *IEEE/ASME Transactions on Mechatronics*, 26(6):3198-3210. https://doi.org/10.1109/TMECH.2021.3055450

Wang N, Su SF, 2021. Finite-time unknown observer-based interactive trajectory tracking control of asymmetric underactuated surface vehicles. *IEEE Transactions on Control Systems Technology*, 29(2):794-803. https://doi.org/10.1109/TCST.2019.2955657

Wang N, Sun Z, Yin JC, et al., 2018. Finite-time observer based guidance and control of underactuated surface vehicles with unknown sideslip angles and disturbances. *IEEE Access*, 6:14059-14070. https://doi.org/10.1109/ACCESS.2018.2797084

Wang N, Gao Y, Zhao H, et al., 2021. Reinforcement learning-based optimal tracking control of an unknown unmanned surface vehicle. *IEEE Transactions on Neural Networks and Learning Systems*, 32(7):3034-3045. https://doi.org/10.1109/TNNLS.2020.3009214

Wang N, Zhang YH, Ahn CK, et al., 2022. Autonomous pilot of unmanned surface vehicles: bridging path planning and tracking. *IEEE Transactions on Vehicular Technology*, 71(3): 2358-2374. https://doi.org/10.1109/TVT.2021.3136670

Wang XM, Song XM, Du LH, 2019. Review and application of unmanned surface vehicle in China. The 5th International Conference on Transportation Information and Safety, p.1476-1481. https://doi.org/10.1109/ICTIS.2019.8883835

Wille KL, Hassani V, Sprenger F, 2016. Modeling and course control of sailboats. *IFAC-PapersOnLine*, 49(23):532-539. https://doi.org/10.1016/j.ifacol.2016.10.490

Xia GQ, Wang XW, Zhao B, et al., 2019. LOS guidance law for path following of USV based on sideslip observer. *Chinese Automation Congress*, p.1312-1316. https://doi.org/10.1109/CAC48633.2019.8996308

Xiao L, Jouffroy J, 2014. Modeling and nonlinear heading control of sailing yachts. *IEEE Journal of Oceanic Engineering*, 39(2):256-268. https://doi.org/10.1109/JOE.2013.2247276

Xu MCX, Wang YT, Han ZQ, et al., 2020. Unmanned surface vehicle path following based on path parameter description. Global Oceans: Singapore–U.S. Gulf Coast, p.1-6. https://doi.org/10.1109/IEEECONF38699.2020.9389063

Zhou ZT, Zhong MY, Wang YQ, 2019. Fault diagnosis observer and fault-tolerant control design for unmanned surface vehicles in network environments. *IEEE Access*, 7:173694-173702. https://doi.org/10.1109/ACCESS.2019.2954352

Electronic supplementary materials

Lemmas S1–S3